AIAA 80-1620R

# Validation of a Wing Leading-Edge Stall Prediction Technique

Jerry Pavelka* and Kenneth E. Tatum†
*McDonnell Aircraft Company, McDonnell Douglas Corporation, St. Louis, Mo.*

**The objective of this research was to design a model wing using previously developed two-dimensional computation techniques for prediction of airfoil leading-edge laminar separation. The wing was designed employing various criteria with the primary objective being to maximize the wing-lift coefficient at which drag rise is caused by leading-edge separation. The model wing was fabricated for test in the McDonnell Douglas Corporation Polysonic Wind Tunnel. The test results compared well with the predicted values and demonstrated substantial improvement in leading-edge separation lift coefficient over a previously tested wing designed without benefit of the laminar separation computation technique.**

## Nomenclature

$b$ = wing span
$c$ = airfoil section chord
$C_D$ = total wing drag coefficient
$C_{D_i}$ = induced drag coefficient
$C_l$ = airfoil section lift coefficient
$C_L$ = total wing lift coefficient
$C_{l_b}$ = airfoil section drag break lift coefficient
$C_{L_B}$ = wing drag break lift coefficient
$C_P$ = pressure coefficient
$M_\infty$ = freestream Mach number
$N$ = induced drag proportionality constant
$Q$ = dynamic pressure, lb/ft$^2$
$RN$ = Reynolds number
$R_\theta$ = Reynolds number based on boundary-layer momentum thickness at separation
$t$ = maximum airfoil section thickness
$x$ = chord distance from airfoil section leading edge
$y$ = spanwise distance from aircraft centerline
$Z$ = maximum airfoil section camber
$\alpha$ = wing angle of attack
$\beta$ = sideslip angle
$\Delta$ = fuselage alone configuration
$\rho$ = airfoil section leading-edge radius

## Introduction

THE desire for high maneuvering capability in advanced high-performance aircraft has encouraged research in high angle of attack aerodynamics. This interest arises not only from a need to increase maximum lift, but also from requirements to reduce drag at high lift coefficients. As a result, research on leading-edge separation and methods of increasing wing drag divergence lift coefficient finds a ready application.

Considerable progress has been made on a method to predict airfoil laminar leading-edge separation through studies of the laminar separation short bubble burst. A schematic representation of the mechanism of bubble formation and burst is shown in Fig. 1. As the airfoil progresses through increasing angles of attack, laminar separation occurs when the adverse pressure gradient in the near vicinity of the airfoil leading edge becomes high enough to detach the laminar boundary layer.

Presented as Paper 80-1620 at the AIAA 7th Atmospheric Flight Mechanics Conference, Danvers, Mass., Aug. 11-13, 1980; received Oct. 8, 1980; revision received March 5, 1981. 

*Technical Specialist, Technology, Aerodynamics. Associate Fellow AIAA.
†Engineer, Technology, Aerodynamics. Member AIAA.

If the Reynolds number is high enough, transition to turbulent flow will occur in the separated shear layer, and the rapid turbulence growth will effect a reattachment of the flow. A short separation bubble is created as shown in Fig. 1a. Since the bubble is a fraction of 1% of chord in length, the effect of the short bubble on the overall lift and drag is negligible. As the angle of attack increases, the separation point moves forward on the airfoil, the bubble becomes shorter, and the growth of turbulence is not sufficiently fast to permit the flow to reattach. The bubble bursts and the flow either reattaches further downstream creating a long bubble or leaves the airfoil completely (Fig. 1b). If the Reynolds number is low enough, the stability of the laminar boundary layer retards the growth of turbulence after laminar separation occurs. The turbulent growth of the shear layer is too slow to permit reattachment (Fig. 1c), and, in this event, short bubble existence is precluded.

When the short bubble bursts and the separated flow region on the airfoil becomes extensive, the pressure peak collapses, the drag increases, and the lift departs from its normal linear progression with angle of attack.

Herring and Ely[1,2] have developed a procedure for prediction of the occurrence and burst of the laminar short bubble. The procedure includes a correlation with wind tunnel tests of various airfoils, including a test validation of the applicability to swept leading edges. This correlation identifying bubble-burst and hence leading-edge stall conditions is shown in Fig. 2, which was obtained from Ref. 2. The graph identifies the boundary between the existence of the short bubble and bubble burst in terms of geometry and flow properties at the laminar separation point on the airfoil. These flow properties are all analytically defined from airfoil geometry using the Ref. 2 techniques.

The purpose of the study described in this paper was to apply the airfoil section leading-edge stall prediction technique to the design of a model wing and its test in order to validate the applicability of the theory to three-dimensional (3-D) geometries.

## Discussion

### Two-Dimensional Parametric Investigation

A two-dimensional parametric investigation of the bubble-burst phenomenon was conducted in order to provide background data for the design of a full 3-D model scale wing. Holding the chord Reynolds number constant at typical model wing test values, the three prime parameters of the study were: 1) airfoil thickness ratio; 2) leading-edge radius, $\rho$; and 3) chordwise location of maximum camber. The general effect of camber magnitude also evolved during the course of the study. Two symmetric NACA airfoil basic thickness families were selected and the bubble-burst lift coefficient, $C_{l_b}$, was computed for varying geometries. The

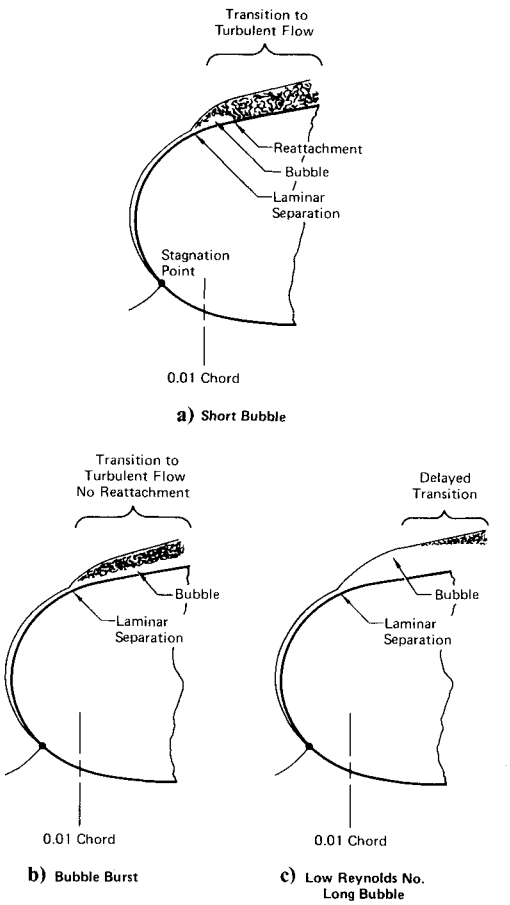


**Fig. 1 Schematic representation of leading-edge laminar separation modes.**

leading-edge radius variation was effected by independently varying either maximum thickness ratio or its location within an airfoil family. The uniform increase of thickness ratio within an airfoil family consistently increased the bubble-burst lift coefficient, $C_{l_b}$. However, the independent variations of thickness and radii showed that radius increase is the predominant effect. In fact, the variation of $C_{l_b}$ with $\rho$ collapses to a single linear curve for each camber distribution regardless of basic thickness airfoil family (Fig. 3). Subsequent study proved that nonzero mean lines merely shift the baseline zero-camber curve and do not affect the linearity or slope.

Figure 3, consisting of typical data extracted from the parametric study, illustrates the effect of two mean-line camber types on the baseline $C_{l_b}$ vs $\rho$ curve. The two curves represent different chordwise maximum camber locations. Increasing the camber magnitude does increase the $C_{l_b}$; however, increases may also be obtained by shifting the location of maximum camber forward.

The significant results of the parametric study are that $C_{l_b}$ is maximized by large leading-edge radius, forward location of maximum camber, and increased magnitude of maximum camber.

Since laminar separation and bubble bursting are viscous phenomena, they are Reynolds number dependent. A lower Reynolds number limit to short bubble occurrence, in terms of the boundary layer momentum thickness Reynolds number at separation, of $R_\theta \simeq 125$ has been postulated by Owen and Klamfer,[3] Gaster,[4] and Ely and Herring.[2] For a chord Reynolds number of 5 million shown on Fig. 3, this $R_\theta$ value of 125 occurs at approximately $\rho/c = 0.0016$ for all the airfoils shown on the figure, and represents the value at which a large, separated region with no short bubble reattachment will occur.

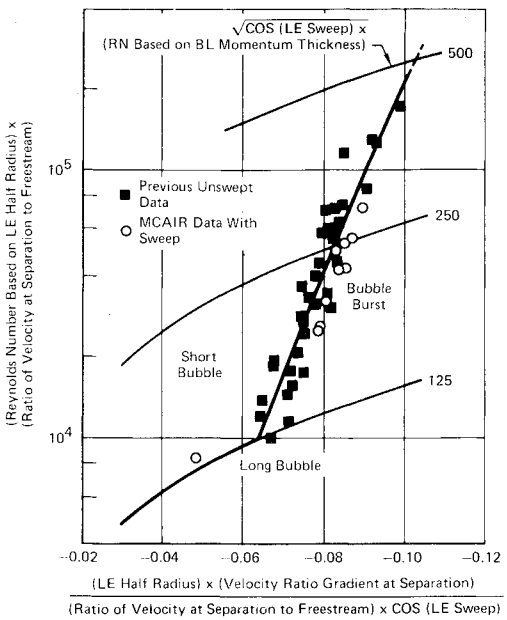


**Fig. 2 Airfoil leading-edge stall prediction.**

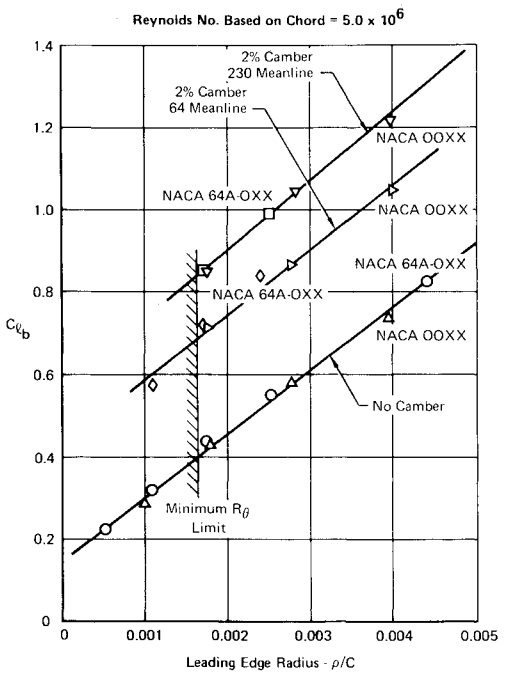


**Fig. 3 Effect of leading-edge radius on laminar bubble burst $C_l$ NACA 64A and 000X airfoils.**

### Scale Model Wing Design

The major purpose of the test program was to validate the applicability of the two-dimensional airfoil leading-edge separation theory to three dimensions. It was also desired to observe to what extent application of the theory to the design of a wing similar to one previously tested could improve on that wing's drag break lift coefficient. Since the previous wing design, $W_{149}$, had been tested in the McDonnell Douglas Corporation Polysonic Wind Tunnel (PSWT) at Mach numbers between 0.6 and 0.95 and at Reynolds number of about 8-9 million/ft, it was desired to design the new wing for test in the same wind tunnel at these conditions. It was also decided to retain the $W_{149}$ planform geometry and to employ the same 0.047 scale model fighter fuselage for wing installation. Figure 4 illustrates the wing planform geometry with its relationship to the fuselage, which constitutes about 30% of the total wing-body semispan.

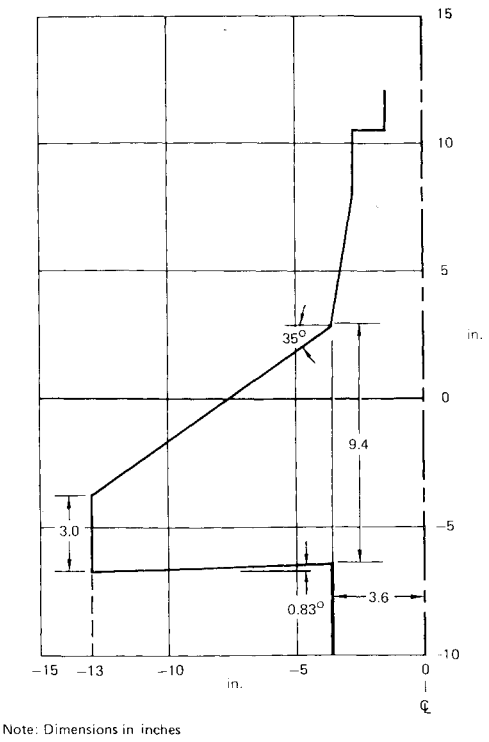


Note: Dimensions in inches

**Fig. 4 Wing $W_{153}$ planform geometry.**

The laminar short bubble wing, $W_{153}$, design criteria is as follows:

1) Use planform of previous wing design ($W_{149}$).
2) Maximize wing $C_L$ for initial section bubble burst.
3) Maximize leading-edge radius at fixed maximum $t/c$.
4) Select type of camber distribution to increase crest sweep.
5) Subcritical flow at $M_\infty = 0.6$ and high lift coefficient.
6) Maximum camber and twist adjusted for high drag divergence Mach at low lift coefficient.

The prime requirement was to maximize the drag break lift coefficient employing the prediction techniques of Refs. 1 and 2. Since the two-dimensional parametric study showed the strong influence of increased radius on the short laminar bubble burst lift coefficient, it was decided to use a modified NACA 0006 airfoil section. The section modification involved thickening it linearly aft of the maximum thickness to provide a trailing-edge thickness for installation of static pressure taps at the trailing edge. The forward location of the maximum thickness of the NACA 000X family provides those airfoils with a large leading-edge radius for a specified thickness. Since it was felt unnecessary and unrealistic to design a new airfoil with a larger leading-edge radius, this NACA 0006 selection was considered adequate. The two-dimensional parametric study also showed the favorable influence of forward maximum camber location on bubble burst. The NACA 230 mean-line camber was chosen for the wing root section because of its 15% chord location of the maximum camber. A more forward location might be desirable, but would fall outside of the applicability of the prediction technique. The prime objective was to obtain the best possible drag break lift coefficient at 0.6 Mach number and retention of the NACA 230 mean line throughout the wingspan would best attain this objective. However, it was decided to compromise somewhat to improve the low lift coefficient compressibility drag rise Mach number. This was done by providing an additional sweep of the wing crest line through selection of an aft-cambered mean line for the wing tip. The one selected was the NACA $a = 0.9$ mean line which has a maximum camber location a little over 50% of the chord.

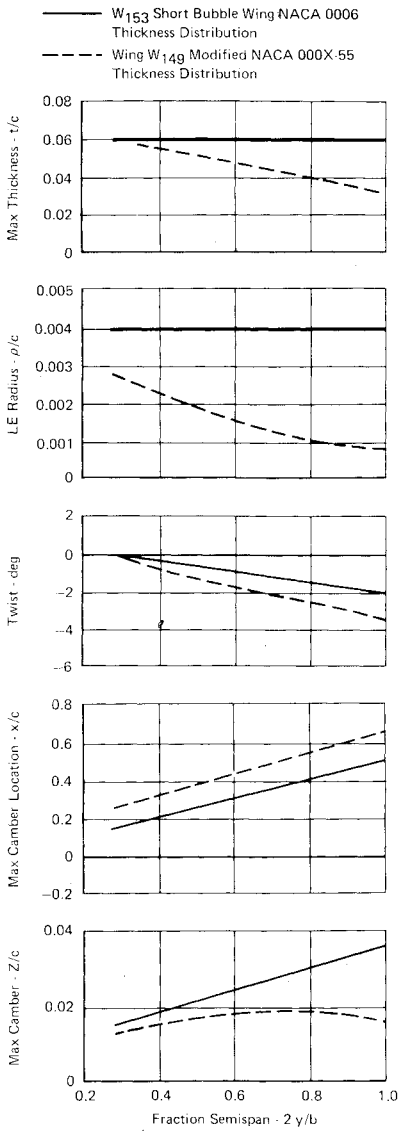


**Fig. 5 Wings $W_{153}$ and $W_{149}$ design geometry characteristics.**

A McDonnell Aircraft Company computer code which employs a vortex lattice approach modified to include the effect of wing thickness was used to design the wing. The computer program permits the calculation of wing lift coefficient from the input wing geometry and section maximum lift or section bubble-burst limits. The program includes compressibility corrections and a routine for computing the local Mach number normal to the crest line for input lift coefficient and Mach number. This feature was used to compute the drag divergence Mach number. The wing geometry was further defined by specification of the wing root and tip maximum camber and the wing tip twist assuming a linear variation from root to tip. An interpolation feature of the computer code permits the definition of intermediate wingspan station section geometries. With these computer code features, it was possible to systematically vary wing root and tip maximum camber and wing tip twist. The selected wing possessed the highest lift coefficient for incipient leading-edge stall at some span station for completely subcritical flow at a freestream Mach number of 0.6. The selection was somewhat compromised to assure a reasonably high drag divergence Mach number at low lift coefficients. The computed drag break lift coefficient for this wing was 0.84 at $M_\infty = 0.6$. The wing geometry arrived at employing these procedures is shown in Fig. 5 and is labeled $W_{153}$. Also shown for reference is the basic $W_{149}$ wing previously tested. The significant departures of the newly designed wing from that of the reference $W_{149}$

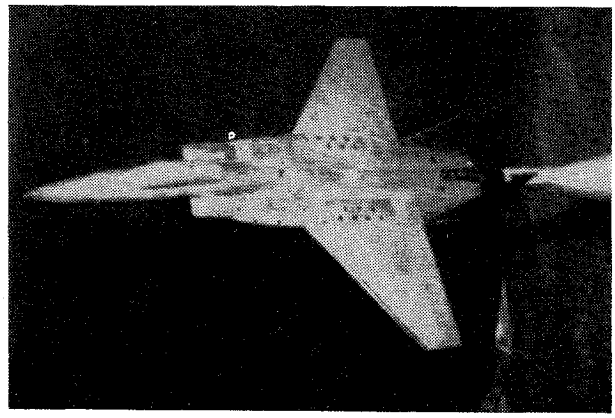

Fig. 6 4.7 % scale fighter model in the PSWT with wing $W_{153}$.

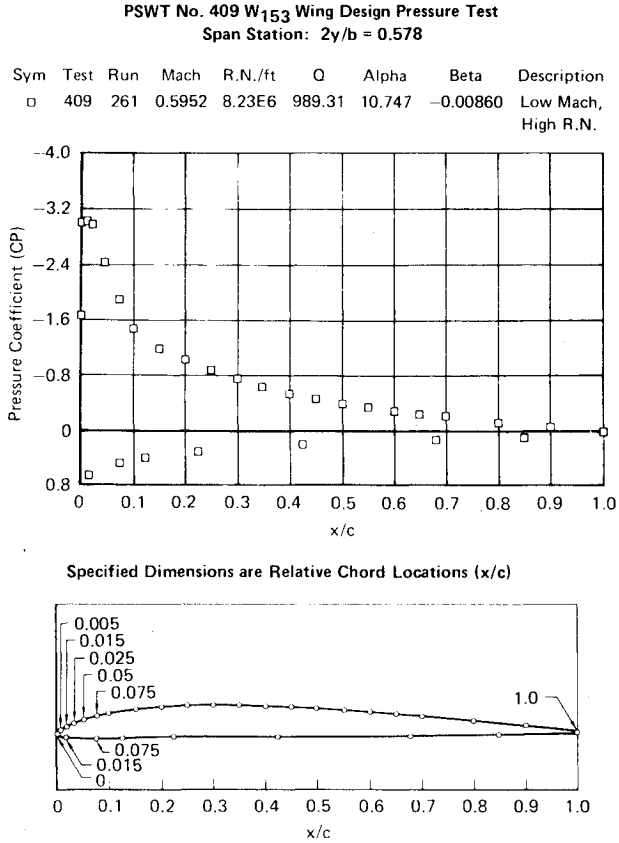


Fig. 7 Typical airfoil section of wing $W_{153}$ showing pressure instrumentation locations, emphasizing leading-edge distributions.

are the increased leading-edge radius particularly at the wing tip, the forward shift in the location of maximum thickness, and the substantial increase in wing tip maximum camber.

### Wind Tunnel Test

The $W_{153}$ short bubble wing design was fabricated within small tolerances to be tested on a 0.047 scale sting-mounted high-performance fighter fuselage model including flow-through inlets and twin vertical tails (no horizontal tail). While standard grit was applied to the fuselage nose, inlet, and tail surfaces to fix transition, the new wing was tested clean to allow free transition as predicted by the laminar bubble theory. The baseline wing, $W_{149}$, was tested with standard grit at 5% chord as in previous tests in an effort to verify the existing data. All tests were conducted in the McDonnell Douglas Corporation 4×4 ft polysonic wind tunnel in St. Louis, Missouri and are described in more detail in Refs. 5 and 6.

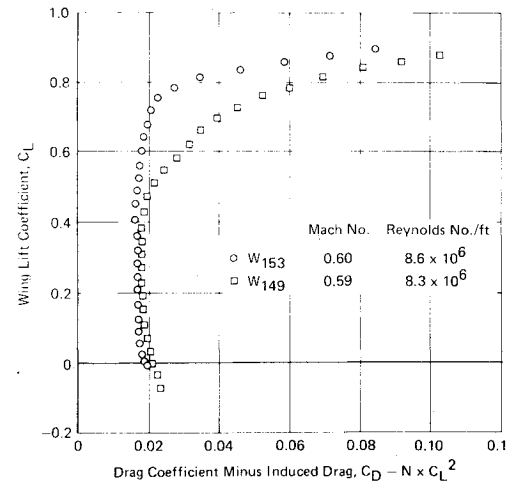


Fig. 8 Test drag comparison of $W_{153}$ and $W_{149}$ wings.

The force and moment runs were conducted at high tunnel Reynolds numbers of 8-9 million/ft over a Mach range of 0.5 to 1.6. This study addresses only the subsonic results. The upper range of the tunnel Reynolds number capability was desired to avoid the low Reynolds number long/short bubble boundary. Three model configurations were tested for force and moment characteristics: 1) fuselage alone, Δ; 2) Δ plus wing $W_{149}$; and 3) Δ plus wing $W_{153}$. Limited subsonic runs were conducted on configurations 1 and 2 as retests to verify existing data. Figure 6 shows configuration 3 mounted in the wind tunnel.

For the pressure distribution portion of the test, the left-wing panel of $W_{153}$ was instrumented with 135 pressure orifices at six span stations on both upper and lower wing surfaces. Figure 7 shows a typical section profile for $W_{153}$ noting the locations of the orifices. A typical pressure distribution plot for the same section is also shown with the plot legend noting the test conditions. Only configuration 3 was pressure tested, and data were obtained at high tunnel Reynolds number (8-9 million/ft) and 0.6 and 0.9 Mach number for angles of attack between 0 and 20 deg (0 deg sideslip).

Flow visualization experiments were also conducted on configuration 3 in an effort to observe the appearance and growth of leading-edge separation regions. A mixture of titanium oxide and silicone oil was painted in a uniform band spanwise along the wing leading edge prior to testing. One angle of attack setting was analyzed per flow visualization run and photographs of resultant flow patterns were made after tunnel shutdown. The runs were at high Reynolds number and 0.6 Mach number.

### Data Analysis

The analysis of the force and moment data is directed toward determination of the first substantial departure of the data from the theoretical variation of inviscid attached flow (drag break). The viscous effects of an attached boundary layer cause some departure from theory, but usually of much smaller magnitude than the substantial change caused by flow separation. Examination of the lift data of wings $W_{149}$ and $W_{153}$ show extensive regions of linear behavior of lift coefficient with respect to angle of attack. Departures from linearity occur very gradually and at lift coefficients of 0.7 and above for Mach = 0.6. The pitching moment coefficient vs angle of attack curves for the two wings are also very similar with large regions of linearity. Thus, in neither the lift nor the moment data are there any abrupt changes indicative of sudden flow separation.

Examination of the drag coefficient variation does show a difference in the behavior of the two wings. The standard drag polars of the wings tend to merge at low lift coefficients and diverge as lift increases.

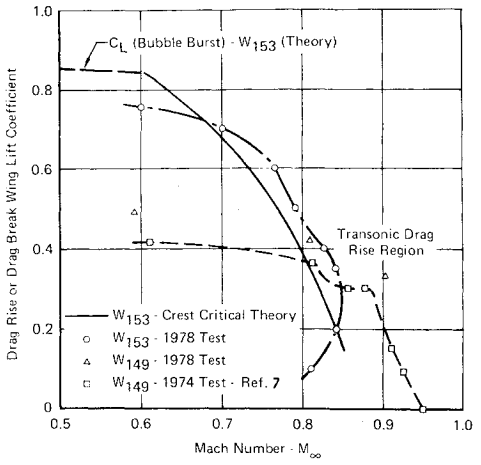


**Fig. 9 Summary of test results on short laminar bubble wing design, $W_{153}$.**

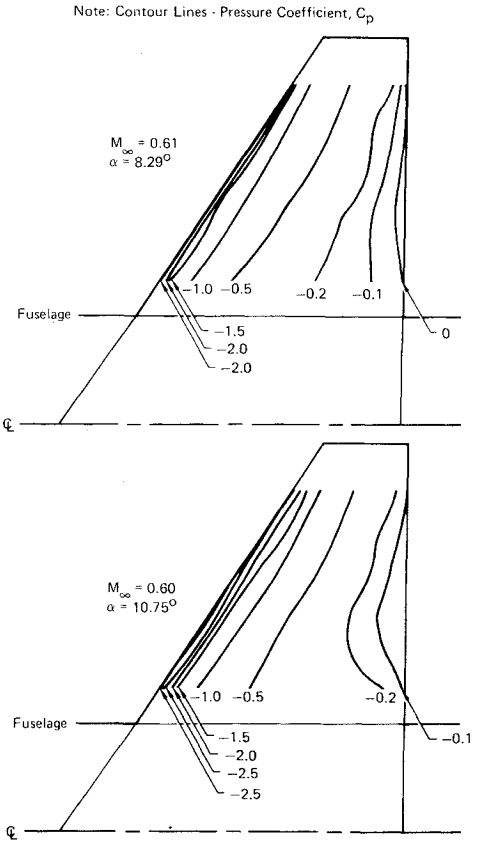


**Fig. 10 Pressure contours on upper surface of wing $W_{153}$ at $M_\infty = 0.6$ for two angles of attack.**

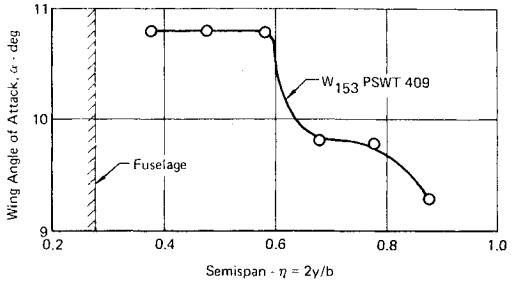


**Fig. 11 Spanwise location of leading-edge stall vs wing angle of attack, $M_\infty = 0.6$.**

The induced drag of a wing is proportional to the square of the lift for attached flow. The proportionality constant is computed as a function of wing planform. The subtraction of the theoretical induced drag from the total drag $C_D$ yields the additional profile drag. Normally, the additional profile drag is near constant with lift coefficient for a given wing geometry. However, when separation occurs, the wing profile drag increases. Figure 8 shows the additional profile drag polars of wings $W_{149}$ and $W_{153}$ at 0.6 Mach number. On these curves, definite departures or breaks in the profile drag behavior are evident. These drag breaks indicate the lift coefficient at which extensive separation occurs, and the improvement of $W_{153}$ over $W_{149}$ (0.47 to 0.75) in the drag break lift coefficient, $C_L$, is obvious. The improvement is attributable to application of the theory to the new wing to assure short bubble formation and delay of burst to high lift coefficients. On the other hand, $W_{149}$ has been theorized[7] to incur initial separation of the long bubble type. Short bubble separation apparently never occurs on $W_{149}$.

While the theoretical design point of $C_{L_B} = 0.84$ at Mach $= 0.6$ was not achieved, $C_{L_B} = 0.75$ from experiment, the improvement through use of the new theory for leading-edge laminar short bubble separation and burst was substantial. Analysis of the force data over the entire subsonic Mach range yields the boundary at which drag rise begins. Figure 9 compares this experimental boundary with the theoretical boundaries for $W_{153}$ computed from the subsonic bubble-burst theory and transonic crest critical drag divergence theory. Also shown is the experimental drag rise boundary for $W_{149}$ with data from two tests of the wing. The significant improvement of $W_{153}$ over $W_{149}$ for subsonic drag break is obvious.

The reduction in the drag divergence Mach number at low lift coefficients is due to the compromise in favor of leading-edge separation characteristics. The large amount of leading-edge camber in $W_{153}$ was needed to attain high lift coefficients, but the resulting wing root forward camber apparently caused lower surface flow separation at small angles of attack.

To verify the conclusions derived from the force and moment data, the pressure coefficient distribution on the upper wing surface of $W_{153}$ was analyzed. Figure 10 shows isobar plots of the $W_{153}$ upper surface for the wind tunnel data at 0.6 Mach for two angles of attack—one well below drag break and one just above drag break. The relatively straight isobars illustrate the quality of the flow conditions and the success of the design procedure in achieving the spanwise uniformity of flow.

It was desired to obtain direct verification of the wing lift coefficient at which leading-edge separation occurs from examination of the wing pressure distribution data. The model scale did not permit a sufficient fineness of pressure orifices located in the vicinity of the wing leading edge to specifically define the development and burst of the minute short laminar separation bubble by observation of pressure distributions. Some approximate verification is possible, however. Examination of the drop in peak velocity or suction pressure in the vicinity of the leading edge at various wingspan stations, as angle of attack is increased, provides information on when the leading edge stalls at a specific span station. The following analysis of the pressure data discusses the spanwise progression of the drop of leading-edge peak velocity and the wing angle of attack and lift coefficients at which each span station experiences the drop.

Figure 11 shows the variation of $W_{153}$ wing angle of attack at which leading-edge stall occurs at various semispan stations for a Mach number of 0.6. The wing angle varies between the narrow limits of 9-11 deg for stall at the various span stations. In order to correlate with wing lift coefficient drag break obtained from the force test data, the data of Fig. 11 have been recast in terms of wing lift coefficient rather than angle of attack. Figure 12 shows the comparison of the test value of stall spanwise location at various lift coefficients vs the theory for

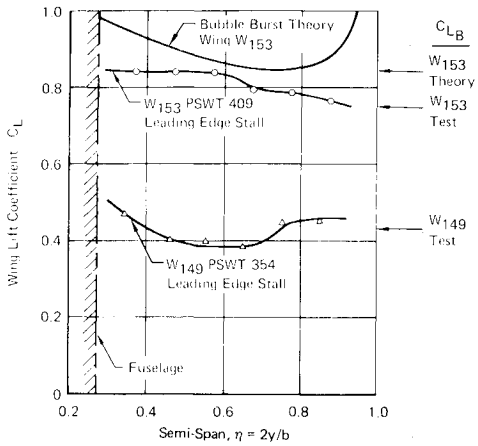


**Fig. 12 Spanwise location of stall vs wing lift coefficient, $M_\infty = 0.6$.**

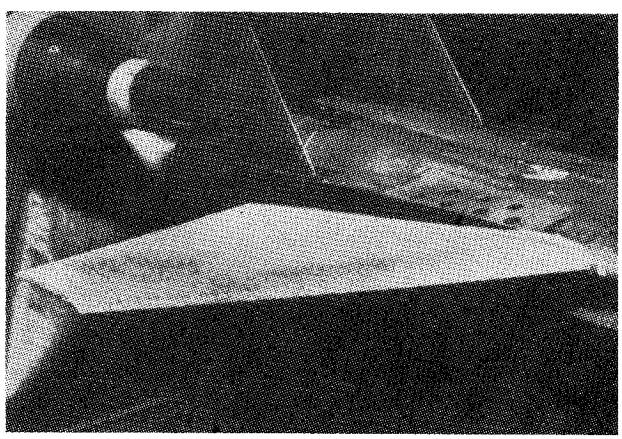

**Fig. 13 Flow visualization photograph of $W_{153}$ wing showing attached flow prior to separation Mach 0.6, $\alpha = 8.3$ deg.**

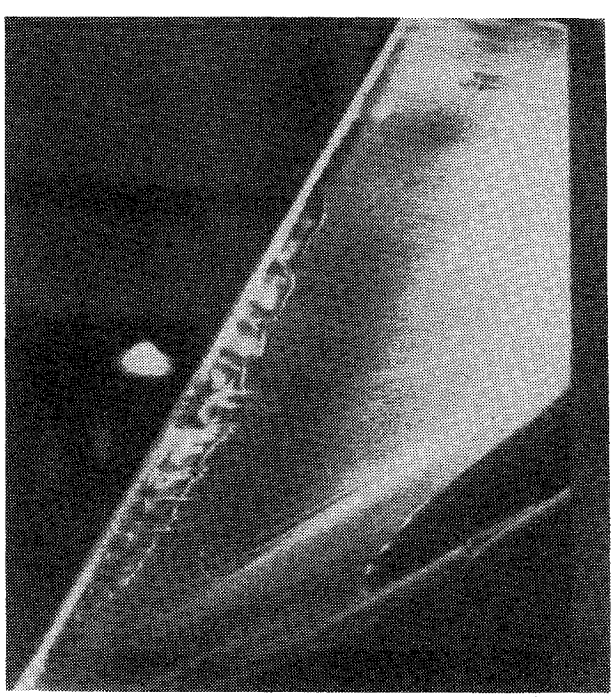

**Fig. 14 Flow visualization photograph of $W_{153}$ wing showing long bubble leading-edge separation region Mach 0.6, $\alpha = 10.5$ deg.**

the $W_{153}$ wing. Also shown are the test results for the basic $W_{149}$ wing. The improvement of the newly designed $W_{153}$ wing is apparent. Also shown on Fig. 12 are the force test and theoretical values of the wing lift coefficient at drag break for wing $W_{153}$ and the force test value for $W_{149}$. It can be seen that the $W_{153}$ test values of wing lift coefficient for stall approach the theoretical values at about the midpoint of the exposed wing semispan. The earlier stall of the outboard wing stations indicated by test results is probably the result of tip effects not accounted for by the application of the theoretical procedure. It is this earlier stall of the tip sections that account for the slightly lower wing drag break lift coefficient of the test data compared to the theory.

An additional qualitative substantiation of the leading-edge separation analysis of the force, moment, and pressure data is evident in the flow visualization results on $W_{153}$. Flow patterns observed in these experiments at angles of attack less than 9 deg (Fig. 13) show smooth streamlines proceeding aft from the leading edge typical of completely attached flow or a short separation bubble too small to be noticeable. Figure 14, however, observed at a 10.5 deg angle of attack shows a distinct region near the leading edge where streamlines have disappeared. This region appears to be a long separation bubble occurring after the short laminar bubble burst followed by reattachment and smooth attached streamlines proceeding onto the trailing edge. The 10.5 deg angle of attack corresponds closely to the angle at which leading-edge pressure loss first covers the entire semispan, as shown by the pressure analysis.

## Conclusions

A scale model wing was designed for testing at subsonic and transonic speeds in order to maximize the wing lift coefficient for leading-edge stall at wind tunnel test Reynolds number. The wind tunnel data obtained included force and moment data, wing pressure distributions, and flow visualization photographs. All phases of the test results substantiated the applicability of the leading-edge stall prediction technique toward design of a scale model wing. Test results agreed well with the predictions. Comparison of the test results with a wing of similar planform, but not designed with the benefit of the new prediction technique, showed substantial drag break lift coefficient improvements.

## References

[1] Herring, R.N. and Ely, W.L., "Improved Prediction of Laminar Leading Edge Separation," NASA Conference Publication 2045, Paper 20 Advanced Technology Airfoil Research, March 1978.

[2] Ely, W.L. and Herring, R.N., "Laminar Leading Edge Stall Prediction for Thin Airfoils," AIAA Paper 78-1222, AIAA 11th Fluid and Plasma Dynamics Conference, Seattle, Wash., July 1978.

[3] Owen, P.R. and Klanfer, L., "On The Laminar Boundary-Layer Separation from the Leading Edge of a Thin Airfoil," Aeronautical Research Council, ARC CP 220, 1953.

[4] Gaster, M., "The Structure and Behavior of Laminar Separation Bubbles," Aeronautical Research Council, ARC R&M No. 3595, 1967.

[5] Pavelka, J. and Tatum, K.E., "Wind Tunnel Force and Moment Test Results of Short Laminar Separation Bubble Wing Design, PSWT Test 406," McDonnell Douglas Corporation, MDC A5730, Aug. 1979.

[6] Tatum, K.E. and Pavelka, J., "Wind Tunnel Pressure Distribution Test Results of Short Laminar Separation Bubble Wing Design, PSWT Test 409," McDonnell Douglas Corporation, MDC A5983, Sept. 1979.

[7] Ely, W.L., "Analysis of the MCAIR Minimum Drag Wing Design Series V Test Data," McDonnell Douglas Corporation, MDC A3740, Oct. 1975.